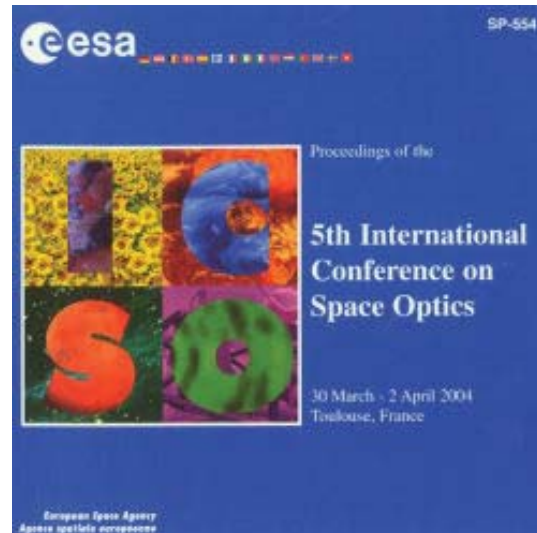


# International Conference on Space Optics—ICSO 2004

Toulouse, France

30 March–2 April 2004

*Edited by Josiane Costeraste and Errico Armandillo*



## *Multiple aperture optical telescopes: some key issues for Earth observation from a GEO orbit*

*L. Mugnier, F. Cassaing et al.*



MULTIPLE APERTURE OPTICAL TELESCOPES: SOME KEY ISSUES FOR EARTH OBSERVATION  
FROM A GEO ORBIT

L. Mugnier, F. Cassaing, B. Sorrente, F. Baron, M.-T. Velluet, V. Michau, and G. Rousset

ONERA/DOTA/CC, BP 72, 92322 Châtillon cedex, France.

ABSTRACT

ONERA is currently conducting a study on the feasibility of an imaging interferometer for Earth observation from a GEO orbit. During this study, some key elements for the definition of such an instrument have been identified and studied. The results obtained so far confirm the applicability of wide-field optical interferometry with a Michelson-type instrument for Earth observation from a GEO orbit.

Key words: Earth observation; interferometry; synthetic aperture optics; cophasing sensor; aperture configuration optimization; optical design; Michelson..

1. INTRODUCTION

ONERA is currently conducting a study on the feasibility of an imaging Multiple Aperture Optical Telescope (MAOT) for high-resolution Earth observation from a geostationary (GEO) orbit. During this study, some key elements for the definition of such an instrument have been identified and studied. They include:

- the optical design of a Michelson-type imaging interferometer.
- the need for a cophasing sensor and the comparison of the concept candidates;
- the definition of system-level parameters such as the minimum collecting surface, with respect to the instrument's mission;
- the optimization of the aperture configuration, i.e., the relative positioning of the individual telescopes that interfere together;

Sections 2 to 5 review the results obtained on these key issues. An important item not mentioned in this list is the definition, manufacturing and operation of a testbed for the selected cophasing sensor; this is discussed in a companion paper [1].

In the following sections, we assume that the images of the instrument will have a pixel size of 1 m and will be Nyquist-sampled at a wavelength of  $\lambda = 0.5\mu\text{m}$ . For a GEO orbit, this leads to a "baseline" (diameter of an equivalent monolithic telescope)  $B \approx 10\text{ m}$ .

2. OPTICAL DESIGN OF A MICHELSON-TYPE IMAGING INTERFEROMETER

Two main kinds of optical design can be considered for a MAOT [2]:

- the "Fizeau" design (Fig. 1a): the aperture segments are portions of a common primary mirror. The length  $L$  is close to the maximum baseline  $B$ ;
- the "Michelson" design (Fig. 1b): independent telescopes are combined by a dedicated telescope. The length  $L$  is close to the telescope diameter  $D$ .

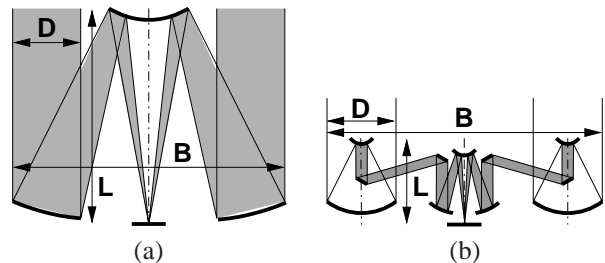


Figure 1. Principle of Fizeau (a) and Michelson (b) MAOTs, with the same maximum baseline  $B$  and sub-aperture diameter  $D$ .

Famous Fizeau designs are each Keck Telescope or the JWST. The Michelson design is mainly used by ground-based stellar interferometers, such as the VLT-I or the Keck-I, with a very diluted aperture and a very small field. But direct wide-field focal-plane imaging with a Michelson MAOT, as illustrated in Fig. 1b, is also possible provided some optical conditions such as homothetic pupil mapping [3] are met. It has been experimentally pioneered by the Multi-Mirror Telescope (MMT) [4], the

Multi-Mirror Telescope Tested (MMTT) [5], the Multi-ap [6]. Very wide field imaging has been validated by simulation with complex designs [7, 8].

The choice between the Michelson and Fizeau designs is a complex system task involving optical design and manufacturing, mechanical design, etc. Such a trade-off can only be performed once the detailed performance of each design is known. Fizeau MAOTs can be considered as masked monolithic telescopes, so they can be simply designed, optimized and characterized with classical optical-design softwares. But to the best of our knowledge, no optical-design software can perform optimization with parallel propagation in several arms. Therefore, the design of a Michelson MAOT is a sophisticated task, which relies heavily on the designer's physical intuition and know-how. Indeed, many specific constraints must be considered simultaneously, as investigated and progressively understood by many authors for astronomy or for wide-field imaging [3, 9, 7, 10, 11, 12].

We investigated in detail the design and optimization of a Michelson MAOT. To this aim, we have developed a computer tool, based on the analytical computation of the aberrations in the sub-telescopes and periscopes of Michelson MAOTs. Such an analytical approach gives more physical insight for each free design parameter and allows one to better control the optimization.

The main result of this study is that a very wide field can be obtained with rather simple designs based on 2-mirrors sub-telescopes, mainly by using a small  $D/B$  ratio [13]. Most other authors propose more complex designs based on at least 3-mirror sub-telescopes. For example, Fig. 2 shows the configuration we used to validate our analytical study by an independent Zemax computation. It is made of 4 Mersenne sub-telescopes (two confocal paraboloïds) combined with a classical 3-mirror Korsch telescope. The linear configuration can be extrapolated to a 2D configuration with same performance, using more telescopes as described in section 5. The Strehl ratio estimated from the wavefront error originating from optical design is larger than 0.95 over a field of 15 000 resolution elements.

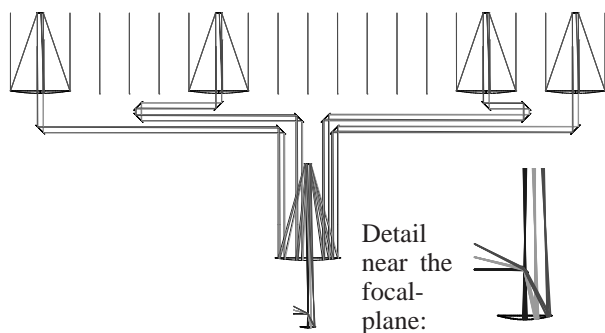


Figure 2. Optical design of a diffraction limited MAOT with a maximum baseline  $B=10$  m and sub-telescopes with diameter  $D=1$  m.

### 3. COPHASING SENSOR

For correct performance, the aperture of an imaging instrument must be phased to a small fraction of the wavelength. For a 10 m aperture diameter in the visible as considered here, this leads to a figure control better than 1 part in  $10^8$ , which can not be met passively. Active or adaptive optics (AO) is a technique based on the closed-loop control of optical actuators from measurements performed by a wavefront sensor, to compensate in real-time for static or evolving aberrations. AO has been successfully validated on ground (see e. g. [14]) and is now considered for monolithic telescopes to make on-orbit correction of thermo-mechanical drifts. AO is unavoidable for future high-resolution space-borne MAOTs, as considered here, for which the main errors are the relative piston and tip/tilt between the apertures deployed after launch. Even if the instrument can be stabilized by a complex internal metrology, we believe that an external sensor, based on the analysis of the observed scene, is required to cancel drifts induced by differential paths [15, 2].

Measurement of tip/tilt, or of higher-order aberration modes, is now a well established technique for monolithic telescopes, even on very extended objects such as the Earth seen from space [16]. Piston measurement has also been widely studied for metrology sensors, and piston compensation of distant telescopes has been demonstrated with non-cooperative sources on the ground [17, 18]. But for most of these devices based on a pupil-plane combination, the contrast of interference fringes strongly decreases as the object extension increases, which makes them useless on very extended scenes. To overcome this problem, specific kinds of fringe sensors have been proposed.

A first solution is spatial filtering (SF) with a field stop in each sub-telescope, to extract a spot from the scene [19]. The main drawback of this technique proposed for Sun observation is that since the field stop dimension must be close to the sub-aperture resolution, only a very small amount of the scene flux is used, which is not acceptable for Earth observation. In addition, to ensure a high fringe visibility, a high pointing accuracy must be achieved on each telescope and the ratio  $B/D$  must be kept small.

Another solution is phase diversity (PD), a focal-plane technique based on the observation of at least two images of the same object to simultaneously solve for the unknown object and phase, as detailed in the companion paper [1]. While originally introduced for monolithic telescopes [20], PD has been extended to MAOTs [21] and has been experimentally validated on a MAOT laboratory breadboard [22]. We have shown that when used for phase measurement, the object can be integrated out of the problem and that this "marginal" PD is more efficient on monolithic telescopes than the classical joint PD methods [23, 24]. Simulations show that marginal PD is also a good solution for MAOT cophasing [25]. An important feature of PD is that complexity is reported on the software: a simple optical hardware theoretically allows the simultaneous measurement of many Zernike modes on a large number of sub-apertures.

Table 1. Summarized comparison between spatial filtering (SP) and phase diversity (PD).

Criterion	SF	PD
Optical setup	complex	<b>simple</b>
$\gg 2$ beams	complex	<b>simple</b>
Coherence constraints	yes	<b>no</b>
High-order modes	no	<b>yes</b>
Data processing	<b>simple</b>	complex

The comparison between these two solutions is summarized in Table 1. Other investigated solutions, such as Hartmann-Shack wavefront sensors with sub-apertures overlapping adjacent MAOT sub-pupils [26], are not suited for large sub-telescope spacing and are not reported here. PD is based on the analysis of the image produced naturally by the MAOT, whereas SF requires a dedicated optical device (inducing differential paths) to insert field stops and implement the pairwise pupil-plane combination, which allows a simple phase computation. A multiple-beam focal-plane combination can also be used with SP, but the data processing is then rather similar to that of PD.

The best solution for Earth observation, according to Table 1, is phase diversity. To test its performance, a prototype sensor and a laboratory bench have been built, as detailed in the companion paper [1].

#### 4. MINIMUM COLLECTING SURFACE

The number of detected photon from a determined area of the earth scene decreases with the altitude of the satellite. This loss can be compensated by a larger collecting area. This is particularly critical for satellites in geostationary orbit. The collecting area must be fixed in order to ensure a sufficient signal-to-noise ratio (SNR) for the data processing of the images. Let  $r$  be the specified SNR per pixel for the detector at the instrument focus. It can be shown that the collecting area  $S_{col}$  is given by :

$$S_{col} = \frac{H^2 r^2}{\tau} g(\Delta\lambda, L_m, p, \dots) \quad (1)$$

where  $H$  is the satellite altitude,  $\tau$  is the exposure time and  $g$  is a function of the characteristics of the scene ( $\Delta\lambda$  spectral bandwidth,  $L_m$  scene luminance,  $p$  pixel size). Eq. 1 shows that as expected the collecting area increases with the instrument altitude. Long exposure times are required to lower  $S_{col}$ . The maximum exposure time  $\tau_{max}$  to be considered is not given by orbiting conditions in the case of a geostationary observation, but by the wavefront error budget  $\sigma_\theta$  allocated to the line-of-sight (LOS) disturbances and by the power spectral density (PSD) of the instrument vibrations  $S_\theta$ . Indeed the vibrations are responsible for a blur effect of the image that increases with the exposure time and degrades the image resolution.

The maximum exposure time  $\tau_{max}$  has been determined by using SPOT5 data for the PSD of the LOS distur-

bances. This PSD has been damped by an active vibration isolation filter in order to obtain a  $f^{-2}$  behavior above 1 Hz [27]. Let  $\sigma_I(\tau)$  be the residual vibration seen by the imaging system for an exposure time  $\tau$ . It can be shown that the expression of  $\sigma_I(\tau)$  is given by :

$$\sigma_I(\tau)^2 = \int_0^{+\infty} \left( 1 - \left( \frac{\sin(\pi f \tau)}{\pi f \tau} \right)^2 \right) S_\theta(f) df \quad (2)$$

where  $f$  is the temporal frequency.  $\tau_{max}$  is obtained when the following condition is fulfilled :

$$\sigma_I(\tau_{max}) = \sigma_\theta \quad (3)$$

For a given SNR and a specification of  $\sigma_\theta = 1.4$  mas for the LOS stabilization (corresponding to  $\lambda/30$  WFE), a collecting area of 60 m<sup>2</sup> has been computed. Such a surface is too high to be integrated in a launch vehicle.

A solution is to compensate the tip-tilt of the instrument using an adequate sensor. Then the disturbances' PSD seen by the imaging system will be a residual PSD after correction.

The principle of the tip-tilt measurement chosen for the study is based on the temporal correlation of sub-images extracted from the focal plane. The detector for the tip-tilt sensor is part of the imaging detector, so the photometric budget of the instrument is not affected by the presence of the sensor. CMOS technology is preferred to a CCD detection despite less technological maturity since windowing read-out is possible while a CCD detector can only be sequentially read-out. The correction is performed using a tip-tilt mirror placed behind the beam-combiner.

The precision of the servo  $\sigma_S$  depends both on the PSD of the disturbances and on the sensor measurement precision [28] :

$$\sigma_S(S_{col}) = f(\text{BP}, \sigma_P, S_\theta(f)) \quad (4)$$

BP is the bandpass of the servo which depends on the read-out frequency  $f_r$  of the detector and increases with the sub-image size in pixel  $n_x \times n_y$ .  $\sigma_P$  is the error introduced in the tip-tilt measurement by the sensor. Its expression is given by [29] :

$$\sigma_P^2 \propto \frac{1}{n_x n_y} \frac{N + n}{N^2} \quad (5)$$

where  $n$  is the detector noise and  $N$  the number of photons detected in the sub-image. Since  $\sigma_P$  depends on  $N$ , it also implicitly depends on  $S_{col}$ .

The goal is now to determine the collecting area for which the servo precision  $\sigma_S = \sigma_\theta$ . Since the tip-tilt is finely corrected, very long exposure time, higher than 1 min, can be considered so that Eq. 1 is fulfilled. The various servo parameters have been tuned in order to lower the collecting area taking into account the state of art of the CMOS detector. Fig. 3 summarizes the results obtained. The curves are characterized by two regimes separated by a minimum. At low bandpass, the images are read-out slowly because  $n_x$  and  $n_y$  are high,  $\sigma_S$  is dominated by

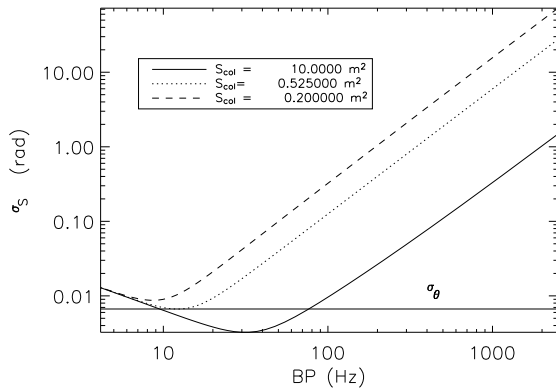


Figure 3. Variation of  $\sigma_I$  versus BP for various collecting areas.

the residual vibrations. In contrary when BP is high, the sub-image contains a small number of pixels, the contribution of the photon noise is dominant.

For an earth scene of a town, sub-images of 300 m length and a bandpass of 10 Hz typically, a minimum collecting area  $S_{col}$  of the order of 1 m<sup>2</sup> has been estimated in the case of a long exposure. The SNR of the images and the budget allocated to the LOS stabilization define the minimum collecting area given above. Because this surface is small, the final collecting area of the instrument will be in fact imposed by the spatial frequency coverage as discussed in section 5 which deals with the aperture configuration optimization.

We thus demonstrated that a pointing control system employing autocorrelation of sub-images meets the requirements for the wavefront error budget allocated to the LOS in geostationary observation. Such system allows also a significant relaxation of the collecting area leading to long exposure observation.

## 5. APERTURE CONFIGURATION OPTIMIZATION

### 5.1. Introduction

The relative arrangement of the elementary telescopes (the so-called aperture configuration, or pupil configuration) is a key aspect of the design of an interferometer. There is an abundant literature on this subject in radio astronomy (see, in particular, the pioneering work of Moffet [30] and of Golay [31], and the papers by Cornwell [32] and by Lannes *et al.* [33]). More recently, many papers have discussed this subject with respect to optical instruments (see, e.g., [34] for a review and extensive references). In this paper, we focus on imaging MAOTs, which form images of the observed object in a focal plane, as opposed to optical interferometers such as the VLTI, which provide only visibilities (Fourier samples of the observed object).

Early papers (before 1990) on the aperture configuration optimization for MAOTs often used various criteria based on the shape of the point spread function (PSF) such as the full width at half maximum, the encircled energy, and the side-lobe level. In these papers the best PSF is implicitly taken as that of the full-aperture telescope, which also implicitly means that the recorded image is considered to be used without an image restoration.

Nevertheless, it has already been pointed out in 1986 that the choice of an optimal aperture configuration should be based on Fourier domain considerations [35]. And we believe that the image restoration step should be regarded as part of the observation system, the first part being the instrument itself. Some papers dealing with the aperture configuration optimization of a MAOT do take a quality criterion based on the uniform filling of the spatial-frequency plane [36, 37] (the so-called  $u-v$  plane) or on the maximization of the contiguous central core diameter of the optical transfer function, [38] (OTF) rather than on the shape of the PSF, but this uniformity is not very precisely defined. Also, the frequency coverage given by the elementary telescopes—which can be an advantage of optical wavelengths over radio wavelengths—is rarely [39, 40] taken into account.

The purpose of this paper is to derive a criterion for aperture configuration optimization of imaging MAOTs under constraints such as the total collecting surface and the system complexity (e.g., the number of apertures or their sizes).

### 5.2. Optimality criterion for aperture configuration

We consider an imaging MAOT whose field aberrations can be neglected. The recording process is modeled as:

$$i = h * o + n \quad (6)$$

where  $o$  is the observed object (scene),  $i$  is the recorded image,  $n$  is an additive noise and  $*$  denotes a convolution.

As mentioned in the introduction, the quantity of utmost interest is not the raw image, but rather the object that can be estimated from this image. Here, we choose to perform the restoration by means of the Wiener filter, because it is optimal in the mean-square sense in the class of linear filters and because it lends itself to analytical calculations. The estimated object is then, in Fourier space:

$$\tilde{o}_e = \frac{\tilde{i} \tilde{h}^*}{|\tilde{h}|^2 + S_n/S_o} \quad (7)$$

where  $\tilde{\cdot}$  denotes Fourier transformation and  $S_n$  and  $S_o$  are the power spectral densities (PSD) of the noise and of the object respectively.

The restoration error  $\epsilon$  can be defined as the RMS difference between the original object  $o$  and its estimate  $o_e$ :  $\epsilon^2 \triangleq \sum_{k,l} |o_e(k,l) - o(k,l)|^2$ . Thanks to Parseval's theorem, this error can also be written:

$$\epsilon^2 = \iint |\tilde{o}_e - \tilde{o}|^2(\nu_x, \nu_y) d\nu_x d\nu_y. \quad (8)$$

For the design of an operational system, there exists a frequency domain of interest  $\mathcal{D}$  given by the resolution needed for the considered mission. For simplicity we consider that this domain is a disk of radius  $\nu_{\max} = B/\lambda$ , called the maximum frequency of interest. As a consequence, the metric of interest is rather:

$$\epsilon_{\mathcal{D}}^2 = \iint_{(\nu_x, \nu_y) \in \mathcal{D}} |\tilde{o}_e - \tilde{o}|^2(\nu_x, \nu_y) d\nu_x d\nu_y. \quad (9)$$

The approach we take is that of experiment planning: the optimal aperture configuration is the one that yields the smallest error, on average for a class of objects and a large number of noise outcomes. Let  $\epsilon_{\mathcal{D}}$  be this average error, plugging Eqs. (6) and (7) into Eq. (9) and averaging the latter yields:

$$\begin{aligned} \epsilon_{\mathcal{D}}^2 &\triangleq \langle \epsilon_{\mathcal{D}}^2 \rangle_{o,n} \\ &= \iint_{(\nu_x, \nu_y) \in \mathcal{D}} \frac{S_n(\nu_x, \nu_y) d\nu_x d\nu_y}{|\tilde{h}|^2(\nu_x, \nu_y) + S_n/S_o(\nu_x, \nu_y)} \end{aligned} \quad (10)$$

For a white noise, this simplifies further:

$$\epsilon_{\mathcal{D}}^2 \propto \iint_{(\nu_x, \nu_y) \in \mathcal{D}} \frac{d\nu_x d\nu_y}{|\tilde{h}|^2(\nu_x, \nu_y) + S_n/S_o(\nu_x, \nu_y)}. \quad (11)$$

This result extends earlier work based on the same approach[34] in that it uses a Wiener filter instead of an inverse filter truncated to the maximum frequency of interest  $\nu_{\max}$ . In particular, if we consider that the SNR is high below this frequency ( $S_n/S_o \rightarrow 0$ ) then Eq. (11) reduces to

$$\epsilon_{\mathcal{D}}^2 \propto \iint_{(\nu_x, \nu_y) \in \mathcal{D}} \frac{1}{|\tilde{h}|^2(\nu_x, \nu_y)} d\nu_x d\nu_y, \quad (12)$$

which is equivalent to Eq (19) of [34].

The numerical minimization of Eq. (11) with respect to the positions of the individual telescopes has been implemented by means of a conjugate-gradient method and yields the optimal configurations, for a given number of sub-apertures of a given size.

### 5.3. Extension to a rotating instrument

In this subsection, we consider that the instrument is rotating, so as to synthesize an aperture in time. This is a natural and effective way to reduce the size and number of the sub-apertures, as noted by Guyon[41].

If we assume that the PSFs of all  $L$  sub-apertures are identical and that these PSFs have rotational symmetry, then the long-exposure PSF and the long-exposure Optical Transfer Function of the instrument can be derived analytically. For an integer number of revolutions of the instrument, the latter reads:

$$\begin{aligned} \tilde{h}(\nu_x, \nu_y) &= \tilde{h}_o(\nu_x, \nu_y) \star \frac{1}{2\pi\sqrt{\nu_x^2 + \nu_y^2}} \times \\ &\sum_{l=1}^L \sum_{l'=1}^L \delta(\sqrt{\nu_x^2 + \nu_y^2} - \rho(l, l')) \end{aligned} \quad (13)$$

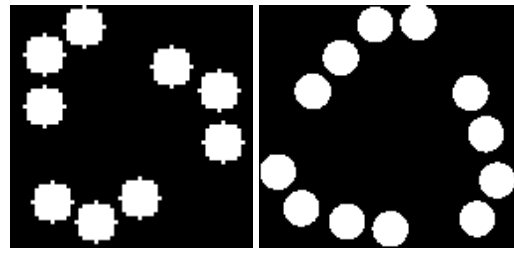


Figure 4. Optimal aperture configurations obtained with 9 (left) and 12 telescopes (right).

where  $\tilde{h}_o$  is the instantaneous OTF of a sub-aperture,  $\rho(l, l')$  is the  $l-l'$  baseline, *i.e.*, the Euclidean distance between telescopes  $l$  and  $l'$  (expressed in number of wavelengths), and  $\delta$  denotes Dirac's pseudo-function. This expression shows that the OTF is the circular average of the instantaneous OTF, so that in order to have a reasonable value of OTF at high frequencies the long baselines must be more represented than the short ones.

By replacing the expression of the instantaneous OTF with Eq. (13) in the minimization of Eq. (11), one obtains the optimal configurations for a rotating instrument.

### 5.4. Simulations

In the simulations presented here we consider that  $S_n/S_o$  is a constant equal to  $= 10^{-4}$ , which corresponds for instance to recording a point-source with a total flux of  $10^4$  photons and a negligible detector noise. The minimization of the metric defined in Eq. (11) has been performed numerically for various numbers of sub-apertures and various diameters for each sub-aperture, in order to yield the optimal configuration. In practice, because we currently use a gradient-based minimization and the metric has several local minima, it is necessary to use several starting points to get to the global minimum. At this minimum, the value of the metric is very informative, as it gives the average error on the restored object. The diameter of the sub-apertures can be increased until this error is considered reasonable.

Figure 4 shows the configuration optimized in snapshot mode for 9 and 12 sub-apertures. For 12 sub-apertures, the diameter is about 20% smaller than for 9. Complementary simulations show that for a rotating instrument, 7 sub-apertures are enough to obtain a good frequency coverage, even with a diameter 50% smaller than for 9 sub-apertures in snapshot mode.

### 6. ACKNOWLEDGMENTS

We are grateful to V. Bentadj, C. Coudrain, B. Fleury, F. Mendez, J. Montri and L. Rousset-Rouvière for making the BRISE experimental testbed happen. We thank D. Laubier (CNES) for making an independent confirmation of section 2 by computing our design performance with the Zemax software and for providing Fig. 2. Lastly,

we acknowledge DGA/SPOTI for the financial support of this study.

## 7. CONCLUSION

While the testbed results currently remain to be obtained, the remainder of this study confirms the applicability of wide-field optical interferometry with a Michelson-type instrument for Earth observation from a GEO orbit.

## REFERENCES

1. F. Cassaing, B. Sorrente, F. Baron, C. Coudrain, B. Fleury, F. Mendez, V. Michau, L. Mugnier, G. Rousset, L. Rousset-Rouvière, and M.-T. Velluet. Multiple-aperture optical telescopes: cophasing sensor testbed. In *5th International Conference On Space Optics*, volume SP-554, Toulouse, France, 2004. CNES/ESA, ESA.
2. G. Rousset, L. M. Mugnier, F. Cassaing, and B. Sorrente. Imaging with multi-aperture optical telescopes and an application. *C. R. Acad. Sci. Paris, Série IV*, tome 2(1):17–25, January 2001.
3. W. A. Traub. Combining beams from separated telescopes. *Appl. Opt.*, 25(4):528–532, February 1986.
4. D. W. MacCarthy, P. A. Strittmatter, E. K. Hege, and F. J. Low. Performance of the multiple mirror telescope (MMT) VIII. MMT as an optical-infrared interferometer and phased array. In *Advanced technology optical telescopes*, volume 332, pages 57–64. Proc. Soc. Photo-Opt. Instrum. Eng., 1982.
5. C. R. De Hainaut, D. C. Duneman, R. C. Dymale, J. P. Blea, B. D. O’Neil, and C. Hines. Wide field performance of a phased array telescope. *Opt. Eng.*, 34(3):876, March 1995.
6. V. Zarifis et al. The Multi Aperture Imaging Array. In S. Unwin and R. Stachnik, editors, *Working on the Fringe: optical and IR interferometry from ground and space*, volume 194 of *Astron. Soc. Pacific Conf. Series*, pages 278–285, Dana Point, May 1999.
7. T. W. Stuhlinger. All-reflective phased array imaging telescopes. In *International lens design conference*, volume 1354, pages 438–446. Proc. Soc. Photo-Opt. Instrum. Eng., 1990.
8. L. M. Mugnier, F. Cassaing, G. Rousset, and B. Sorrente. Earth observation from a high orbit: pushing the limits with synthetic aperture optics. In *Space-based observation techniques*, Samos, Greece, October 2000. NATO/RTO-SET.
9. L. D. Weaver, J. S. Fender, and C. R. De Hainaut. Design considerations for multiple telescope imaging arrays. *Opt. Eng.*, 27(9):730–735, September 1988.
10. J. E. Harvey and C. Ftaclas. Field-of-view limitations of phased telescope arrays. *Appl. Opt.*, 34(25):5787–5798, September 1995.
11. F. Cassaing. *Analyse d’un instrument à synthèse d’ouverture optique : méthodes de cophasage et imagerie à haute résolution angulaire*. PhD thesis, Université Paris XI Orsay, December 1997.
12. R. L. Lucke. Influence of Seidel distortion on combining beams from a phased telescope array. *Appl. Opt.*, 38(22):4776–4783, August 1999.
13. F. Cassaing, B. Sorrente, B. Fleury, and D. Laubier. Optical design of a michelson wide-field multi-aperture telescope. In *Optical System Design*, volume 5249, Saint-Etienne, France, 2003. Proc. Soc. Photo-Opt. Instrum. Eng.
14. G. Rousset, F. Lacombe, P. Puget, N. Hubin, E. Gendron, T. Fusco, R. Arsenault, J. Charton, P. Gigan, P. Kern, A.-M. Lagrange, P.-Y. Madec, D. Mouillet, D. Rabaud, P. Rabou, E. Stadler, and G. Zins. NAOS, the first AO system of the VLT: on sky performance. In Peter L. Wizinowich and Domenico Bonaccini, editors, *Adaptive Optical System Technology II*, volume 4839, pages 140–149, Bellingham, Washington, 2002. Proc. Soc. Photo-Opt. Instrum. Eng., SPIE.
15. F. Cassaing, L. Mugnier, G. Rousset, and B. Sorrente. Éléments-clés de la conception d’un instrument spatial à synthèse d’ouverture optique. In *International Conference on Space Optics*, Toulouse (France), December 1997. CNES.
16. M.-T. Velluet, V. Michau, and G. Rousset. Wavefront sensors for the active control of earth observation optical instruments. In *International Conference on Space Optics*, Toulouse (France), December 1997. CNES.
17. M. Shao, M. M. Colavita, B. E. Hines, D. H. Staelin, D. J. Hutter, K. J. Johnston, D. Mozurkewich, R. S. Simon, J. L. Hershey, J. A. Hughes, and G. H. Kaplan. The Mark III Stellar Interferometer. *Astron. Astrophys.*, 193:357–371, March 1988.
18. B. Sorrente, F. Cassaing, G. Rousset, S. Robbe-Dubois, and Y. Rabbia. Real-time optical path difference compensation at the Plateau de Calern I2T interferometer. *Astron. Astrophys.*, 365:301–313, 2001.
19. L. Damé. <http://must.aerov.jussieu.fr/>.
20. R. A. Gonsalves. Phase retrieval and diversity in adaptive optics. *Optical Engineering*, 21(5):829–832, 1982.
21. R. G. Paxman and J. R. Fienup. Optical misalignment sensing and image reconstruction using phase diversity. *J. Opt. Soc. Am. A*, 5(6):914–923, 1988.
22. J. H. Seldin, R. G. Paxman, V. G. Zarifis, L. Benson, and R. E. Stone. Closed-loop wavefront sensing for a sparse-aperture, phased-array telescope using broadband phase diversity. In *Imaging technology and telescopes*, volume 4091 of *Proc. Soc. Photo-Opt. Instrum. Eng.*, July 2000.
23. A. Blanc. *Identification de réponse impulsionnelle et restauration d’images : apports de la diversité de phase*. PhD thesis, Université Paris XI Orsay, July 2002.

24. A. Blanc, L. M. Mugnier, and J. Idier. Marginal estimation of aberrations and image restoration by use of phase diversity. *J. Opt. Soc. Am. A*, 20(6):1035–1045, 2003.
25. F. Baron, F. Cassaing, A. Blanc, and D. Laubier. Cophasing a wide field multiple-aperture array by phase-diversity: influence of aperture redundancy and dilution. In M. Shao, editor, *Interferometry in Space*, volume 4852, Hawaii, USA, 2002. Proc. Soc. Photo-Opt. Instrum. Eng., SPIE.
26. A. Schumacher, N. Devaney, and L. Montoya. Phasing segmented mirrors: a modification of the keck narrow-band technique and its application to extremely large telescopes. *Appl. Opt.*, 41(7):1297–1307, March 2002.
27. G. Mosier. Dynamics and controls analysis for the ngst yardstick concept. <http://www.ngst.nasa.gov/doclist/bytitle.html> (NGST website), 1998.
28. V. Michau, G. Rousset, and J.-C. Fontanella. Wavefront sensing from extended sources. In R. R. Radick, editor, *Real Time and Post Facto Solar Image Correction*, number 13 in NSO/SP Summer Workshop Series, pages 124–128, Sunspot, New Mexico, USA, 1992. National Solar Observatory/Sacramento Peak.
29. V. Michau, G. Rousset, and J. C. Fontanella. Wavefront sensing from extended sources. In R. Radick, editor, *Summer workshop*, 13, pages 124–128, Sunspot, New Mexico, USA, 1992. NSO/SP.
30. A. T. Moffet. Minimum-redundancy linear arrays. *IEEE Trans. Antennas Propag.*, AP-16(2):172–175, 1968.
31. M. J. E. Golay. Point arrays having compact, nonredundant autocorrelations. *J. Opt. Soc. Am.*, 61:272–273, 1971.
32. T. J. Cornwell. A novel principle for optimization of the instantaneous Fourier plane coverage of correlation arrays. *IEEE Trans. Antennas Propag.*, AP-36(8):1165–1167, 1988.
33. A. Lannes, É. Anterrieu, L. Kœchlin, and G. Fitoussi. On the concept of field-to-resolution ratio in aperture synthesis. In G. Cerutti-Maori and P. Roussel, editors, *Space Optics 1994: Earth Observation and Astronomy*, volume 2209, pages 402–412. Proc. Soc. Photo-Opt. Instrum. Eng., April 1994.
34. L. M. Mugnier, G. Rousset, and F. Cassaing. Aperture configuration optimality criterion for phased arrays of optical telescopes. *J. Opt. Soc. Am. A*, 13(12):2367–2374, December 1996.
35. J. E. Harvey, A. B. Wissinger, and A. N. Bunner. A parametric study of various synthetic aperture telescope configurations for coherent imaging applications. In R. B. Johnson, W. L. Wolfe, and J. S. Fender, editors, *Infrared, Adaptive, and Synthetic Aperture Optical Systems*, volume 643, pages 194–207. Proc. Soc. Photo-Opt. Instrum. Eng., 1986.
36. A. Labeyrie, G. Lemaitre, and L. Kœchlin. The optical very large array. In Larry D. Barr, editor, *Advanced Technology Optical Telescopes III*, volume 628, pages 323–332. Proc. Soc. Photo-Opt. Instrum. Eng., 1986.
37. M. Faucherre, F. Merkle, and F. Vakili. Beam combination in aperture synthesis from space: Field of view limitations and (u,v) plane coverage optimization. In J.-P. Swings, editor, *New Technologies for Astronomy*, volume 1130 of *Proc. Soc. Photo-Opt. Instrum. Eng.*, pages 138–145, April 1989.
38. J. P. Fitch and T. W. Lawrence. Placement of multiple apertures for imaging telescopes. In Jim B. Breckinridge, editor, *Amplitude and Intensity Spatial Interferometry*, volume 1237, pages 61–69. Proc. Soc. Photo-Opt. Instrum. Eng., 1990.
39. J. E. Harvey and R. A. Rockwell. Performance characteristics of phased arrays and thinned aperture optical telescopes. *Opt. Eng.*, 27(9):762–768, 1988.
40. L. Damé and M. Martić. Study of an optimized configuration for interferometric imaging of complex and extended solar structures. In *Targets for Space-based Interferometry*, volume SP-354, pages 201–208. ESA, December 1992.
41. O. Guyon and F. Roddier. Aperture rotation synthesis: optimization of the (u, v)-plane coverage for a rotating phased array of telescopes. *Pub. Astron. Soc. Pacific*, 113:98–104, January 2001.